Some computational aspects of BEM simulation of cathodic protection systems

J. M. Chuang

Faculty of Engineering, Technical University of Nova Scotia, Halifax, Nova Scotia, Canada

N. G. Zamani

Department of Mathematics, University of Windsor, Windsor, Ontario, Canada

C. C. Hsiung

Faculty of Engineering, Technical University of Nova Scotia, Halifax, Nova Scotia, Canada

(Received July 1986; revised January 1987)

This article discusses the concept of multiple domain and the iterative solution of equations arising in the BEM simulation of cathodic protection systems. The conclusions of the paper are verified by several benchmark problems.

Keywords: BEM, iterative methods, multiple domains, cathodic protection

Introduction

The purpose of this article is to discuss some computational aspects of the boundary element method (BEM) used in the simulation of cathodic protection (CP) systems for corrosion prevention. The two main points discussed are the concepts of multiple imaging and the iterative solution of nonlinear discretized equations. These issues are becoming more and more important as many researchers have become involved with theoretically investigating the simulation of CP systems, and some consulting companies have developed commercial codes along this line.

Naturally, the software developed for commercial purposes must be accurate and efficient to be feasible in industrial applications. Initial attempts in this direction ignored the above issues, but the viewpoint has drastically changed during the past few years.

Since some readers may not be familiar with the design of CP systems, we give a short introduction in the next section. A comprehensive review of the simulation procedure for CP systems is given in Ref. 1.

Cathodic protection

When a metal is placed in a corrosive environment (electrolyte), it tends to ionize and dissolve into the electrolyte. During this reaction, which is an electrochemical process, an electrical field is established. There are two well-known techniques to suppress the corrosion process, both of which are referred as as cathodic protection. The first one is known as the sacrificial anode system, the other as the impressed current system.

In the sacrificial anode case, the metal to be protected is short-circuited to a less noble metal to be corroded at the expense of protecting the more valuable one. In the electrochemical literature, the list of all the metals along with their tendency to corrode (nobleness) is tabulated. According to their terminology, the metal to be protected is known as the cathode and the metal to be sacrificed is the anode. In the impressed current system, the presence of the less noble metal is simulated by an inert electrode that corrodes very little and acts as the anode. This electrode provides sufficient current supplied by a power source to protect the cathode. The design of CP systems, regardless of their type, has to do with lowering the cathode's potential below a critical value known as the protection potential.

The mathematical model that simulates CP systems is based on the concept of conservaton of charge in the body of the electrolyte. Under idealized conditions (homogeneous electrolyte, steady-state situation, etc.), the model reduces to the well-known Laplace equation which then

0307-904X/87/050371-09/$03.00

has to be supplemented by a proper set of boundary conditions. Detailed derivations can be found in Ref. 1. The major reason for the BEM to be quite suitable for the discretization of the model is that the CP system designs require only the potential distribution on the boundary of the structure.

Mathematical formulation

Let Ω be the domain of the electrolyte (two-dimensional for simplicity), bounded by $\Gamma = \Gamma_C \cup \Gamma_A \cup \Gamma_I$, as shown in *Figure 1*. It is assumed that the electrolyte is homogeneous and that Γ_C, Γ_A, and Γ_I are the cathode, the anode, and the insulated surfaces, respectively. A simple argument, based on the conservation of charge, shows that the electrical potential ϕ satisfies the Laplace equation:

$$\nabla^2\phi = 0 \qquad \text{in } \Omega \tag{1}$$

This partial differential equation is supplemented by a combination of the boundary conditions (depending on the situation) described next.

(a) On the cathodic surface Γ_C, the flux proportional to the current density is a nonlinear function of the electrical potential described by

$$\frac{\partial\phi(Q)}{\partial n_Q} = f_C[\phi(Q)] \qquad Q \in \Gamma_C \tag{2}$$

Q is the point under consideration, and n_Q is the outward normal to Γ_C at Q. The function f_C is commonly referred to as the cathodic polarization function.

(b) On the anodic surface Γ_A, in a sacrificial anode system, the flux is also related to ϕ through the anodic polarization function f_A acording to

$$\frac{\partial\phi(Q)}{\partial n_Q} = f_A[\phi(Q)] \qquad Q \in \Gamma_A \tag{3}$$

(c) For an impressed current system, the flux is a specified constant q_A:

$$\frac{\partial\phi(Q)}{\partial n_Q} = q_A \qquad Q \in \Gamma_A \tag{4}$$

(d) At the insulated boundary Γ_I, such as a well-painted surface, the flux is zero:

$$\frac{\partial\phi(Q)}{\partial n_Q} = 0 \qquad q \in \Gamma_I \tag{5}$$

If one is dealing with a nonpolarizable anode, one can assume that the potential ϕ is constant; therefore

$$\phi(Q) = \phi_A \qquad Q \in \Gamma_A \tag{6}$$

Equations (1)–(6), define the boundary value problem associated with a CP system.

In accordance with potential theory[2,3] the potential at an arbitrary point in Ω can be expressed in terms of the potential and its normal derivative on the boundary:

$$2\pi\phi(P) = -\int_\Gamma \left[\phi(Q)\frac{\partial}{\partial n_Q}\left(\ln\frac{1}{r_{PQ}}\right) - \left(\ln\frac{1}{r_{PQ}}\right)q(Q)\right] d\Gamma_Q \qquad P \notin \Gamma,\ p \in \Omega \tag{7}$$

$$\pi\phi(P) = -(P.V.)\int\left[\phi(Q)\frac{\partial}{\partial n_Q}\left(\ln\frac{1}{r_{PQ}}\right) - \left(\ln\frac{1}{r_{PQ}}\right)q(Q)\right] d\Gamma_Q \qquad P \in \Gamma \tag{8}$$

where $q(Q)$ is the flux at Q and the symbol (P.V.)$\int$ is to be interpreted in terms of the Cauchy principal value.

Once the integral equation (8) associated with the boundary conditions (2)–(6) are solved for $\phi(Q)$ and $q(Q)$ on the boundary Γ, the potential at an arbitrary point in the interior of Ω can be calculated from (7).

Several properties of (8) derived from the theory of integral equations[2] will be used and are listed here:

(i) The condition of the solvability of the interior potential problem is

$$\oint q(Q)\, d\Gamma_Q = 0 \tag{9}$$

(ii) If the potential ϕ is specified on Γ (i.e., the Dirichlet boundary condition), the flux q on Γ can be uniquely determined from (8) and it automatically satisfies (9).

(iii) If the flux q is specified on Γ and satisfies equation (9), the solution for ϕ is not unique, but any two solutions differ by a constant.

(iv) Finally, if condition (9) is violated, no solution for ϕ can be obtained.

BEM discretization

The theoretical development of the BEM is well established,[4–7] and only the salient parts are mentioned in this section. For the sake of simplicity, it is assumed that constant panels are employed. The discrete version of the integral equation (8) is as follows:

$$\sum_{j=1}^{N} H_{ij}\phi_j = \sum_{j=1}^{N} G_{ij}q_j \qquad i = 1, 2, \ldots, N \tag{10}$$

where N is the total number of panels and i refers to the field point P.

$$H_{ij} = \begin{cases} \pi + \int_{s_{1j}}^{s_{2j}} \frac{\partial}{\partial n_Q}\left(\ln\frac{1}{r_{PQ}}\right) d\Gamma_Q & \text{if } i = j \\ \int_{s_{1j}}^{s_{2j}} \frac{\partial}{\partial n_Q}\left(\ln\frac{1}{r_{PQ}}\right) d\Gamma_Q & \text{if } i \neq j \end{cases} \tag{11}$$

$$G_{ij} = \int_{s_{1j}}^{s_{2j}} \ln\frac{1}{r_{PQ}}\, d\Gamma_Q \tag{12}$$

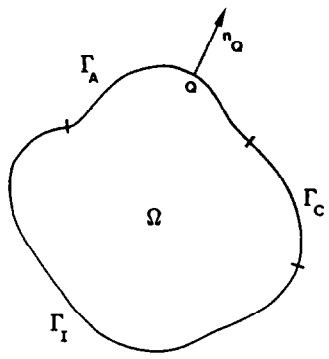

Figure 1 The domain under consideration

The integrals in H_{ij} and G_{ij} can be carried out exactly with a transformation to a local coordinate system along the panel.[4] Equation (10) can be written in detail as the matrix equality

$$\begin{vmatrix} H_{11} & H_{12} & \cdots & H_{1N} \\ H_{21} & H_{22} & \cdots & H_{2N} \\ \vdots & \vdots & & \vdots \\ H_{N1} & H_{N2} & \cdots & H_{NN} \end{vmatrix} \begin{vmatrix} \phi_1 \\ \phi_2 \\ \vdots \\ \phi_N \end{vmatrix} = \begin{vmatrix} G_{11} & G_{12} & \cdots & G_{1N} \\ G_{21} & G_{22} & \cdots & G_{2N} \\ \vdots & \vdots & & \vdots \\ G_{N1} & G_{N2} & \cdots & G_{NN} \end{vmatrix} \begin{vmatrix} q_1 \\ q_2 \\ \vdots \\ q_N \end{vmatrix} \tag{13}$$

Classical potential theory implies that the matrix H is singular, whereas the matrix G is invertible.

Treatment of the corner singularities

It is well known that a corner singularity in the BEM is due to the discontinuity of the normal vector at the corner point; i.e., the normal is simply not defined at the corner point. If the domain of a two-dimensional problem has two vertical boundaries on which the homogeneous Neumann boundary condition, $\partial\phi/\partial n = 0$, is specified (as in *Figure 2*), the eigenfunctions contain a periodic cosine function of x. This can be easily verified by the method of separation of variables. In this situation the domain can be extended perodically to $x = \pm\infty$, and, consequently, the corner singularity disappears. The corresponding scheme in classical potential theory is the infinite series of images.[8] In practical applications the implementation of the infinite periodic domain is impossible. Here, several images of the domain are taken as an approximation, which is called the multiple-domain method (see *Figures 2* and *9*). One can take advantage of the following facts to use multiple domain without solving extra algebraic equations in the discretization process.

(i) Once the boundary element grid is defined in the main domain, the corresponding elements in the image domains can easily be found with the principle of reflection. Notice that the insulating vertical boundaries act as mirrors.
(ii) All the corresponding elements, including those in the main domain, have the same potentials and fluxes as the reflections.

The effectiveness of the suggested multiple-domain technique will be shown in the benchmark problems.

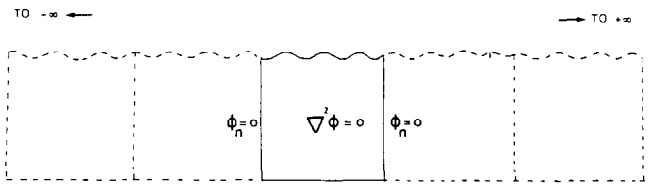

Figure 2 The main domain and the corresponding images

Iteration procedure

The reader is reminded that, due to the nonlinear nature of the boundary conditions, the discretized equation (13) consists of a system of nonlinear equations. In this section the different iteration procedures that can be employed to solve the above system are discussed. For the sake of simplicity we assume that the boundary Γ consists of only three straight panels Γ_A, Γ_C, and Γ_I, as shown in *Figure 3*. Therefore, the boundary conditions associated with the cathode, the anode, and the insulating surfaces are

$$q_C = f_C(\phi_C) \tag{14}$$

$$q_A = f_A(\phi_A) \tag{15}$$

$$q_I = 0 \tag{16}$$

Substituting these expressions in the system (13) gives

$$\begin{vmatrix} H_{11} & H_{12} & H_{13} \\ H_{21} & H_{22} & H_{23} \\ H_{31} & H_{32} & H_{33} \end{vmatrix} \begin{vmatrix} \phi_C \\ \phi_A \\ \phi_I \end{vmatrix} = \begin{vmatrix} G_{11} & G_{12} & G_{13} \\ G_{21} & G_{22} & G_{23} \\ G_{31} & G_{32} & G_{33} \end{vmatrix} \begin{vmatrix} f_C(\phi_C) \\ f_A(\phi_A) \\ 0 \end{vmatrix} \tag{17}$$

In system (17) there are three equations to be solved for the three unknowns ϕ_C, ϕ_A, and ϕ_I. Of course, we could have written the equivalent of system (17) by eliminating the potentials on the cathode and the anode in favor of the fluxes, which yields

$$\begin{vmatrix} H_{11} & H_{12} & H_{13} \\ H_{21} & H_{22} & H_{23} \\ H_{31} & H_{32} & H_{33} \end{vmatrix} \begin{vmatrix} g_C(q_C) \\ g_A(q_A) \\ \phi_I \end{vmatrix} = \begin{vmatrix} G_{11} & G_{12} & G_{13} \\ G_{21} & G_{22} & G_{23} \\ G_{31} & G_{32} & G_{33} \end{vmatrix} \begin{vmatrix} q_C \\ q_A \\ 0 \end{vmatrix} \tag{18}$$

where g_C and g_A are the inverse functions to the cathodic and anodic polarization curves. Here the three unknowns to be determined are q_C, q_A, and ϕ_I. If the latter formulation is employed, the variables q_C and q_A should satisfy the constraint equation.

$$q_C \text{ meas}(\Gamma_C) + q_A \text{ meas}(\Gamma_A) = 0 \tag{19}$$

where "meas" stands for the length or area of the electrodes in 2-D or 3-D cases, respectively. If the constraint equation (19) is violated, the obtained fluxes have neither mathematical nor physical significance. The formulation based on (17) does not have the indicated shortcoming, and it is precisely the reason why we adopt it in the rest of the paper (also see Refs. 9 and 10).

Since the unknown potential ϕ_I can be expressed in terms of the variables ϕ_C and ϕ_A, we can rearrange system (17) to get

$$\begin{vmatrix} H_{11} & H_{12} & -G_{13} \\ H_{21} & H_{22} & -G_{23} \\ H_{31} & H_{32} & -G_{33} \end{vmatrix} \begin{vmatrix} \phi_C \\ \phi_A \\ 0 \end{vmatrix} = \begin{vmatrix} G_{11} & G_{12} & -H_{13} \\ G_{21} & G_{22} & -H_{23} \\ G_{31} & G_{32} & -H_{33} \end{vmatrix} \begin{vmatrix} f_C(\phi_C) \\ f_A(\phi_A) \\ \phi_I \end{vmatrix} \tag{20}$$

Multiplying both sides of (20) by the inverse of the matrix appearing on the right side of the same equation gives

$$\begin{vmatrix} A_{11} & A_{12} & A_{13} \\ A_{21} & A_{22} & A_{23} \\ A_{31} & A_{32} & A_{33} \end{vmatrix} \begin{vmatrix} \phi_C \\ \phi_A \\ 0 \end{vmatrix} = \begin{vmatrix} f_C(\phi_C) \\ f_A(\phi_A) \\ \phi_I \end{vmatrix} \tag{21}$$

Consequently, we can concentrate on developing iteration methods for the partitioned version of (21), namely,

$$\begin{vmatrix} A_{11} & A_{12} \\ A_{21} & A_{22} \end{vmatrix} \begin{vmatrix} \phi_C \\ \phi_A \end{vmatrix} = \begin{vmatrix} f_C(\phi_C) \\ f_A(\phi_A) \end{vmatrix} \tag{22}$$

The three methods to be discussed for the iterative solution of system (22) are (a) Jacobi's method, (b) Gauss–Siedel method and (c) Newton–Raphson method.

Jacobi's method

System (22) is iterated according to

$$\phi_C^{K+1} = \frac{1}{A_{11}} \left[-A_{12}\phi_A^K + f_C(\phi_C^K) \right] \tag{23}$$

$$\phi_A^{K+1} = \frac{1}{A_{22}} \left[-A_{21}\phi_C^K + f_A(\phi_A^K) \right] \tag{24}$$

where K and $K+1$ denote the Kth and $(K+1)$st iterations, respectively. The iteration procedure is as follows:

(i) Guess ϕ_C^K and ϕ_A^K.
(ii) Calculate $f_C(\phi_C^K)$ and $f_A(\phi_A^K)$ from the cathodic and anodic polarization curves.
(iii) Find ϕ_A^{K+1} and ϕ_A^{K+1} from equations (23) and (24).
(iv) Repeat steps (i)–(iii) until convergence is achieved.

Gauss–Siedel method

System (22) is iterated according to

$$\phi_C^{K+1} = \frac{1}{A_{11}} \left[-A_{12}\phi_A^K + f_C(\phi_C^K) \right] \tag{25}$$

$$\phi_A^{K+1} = \frac{1}{A_{22}} \left[-A_{21}\phi_C^{K+1} + f_A(\phi_A^K) \right] \tag{26}$$

The iteration procedure is exactly as in steps (i)–(iv) of Jacobi's method.

Newton–Raphson method

By introducing the functions $F_i(\phi_C, \phi_A)$, defined as

$$\begin{vmatrix} F_1(\phi_C, \phi_A) \\ F_2(\phi_C, \phi_A) \end{vmatrix} = \begin{vmatrix} f_C(\phi_C) \\ f_A(\phi_A) \end{vmatrix} - \begin{vmatrix} A_{11} & A_{12} \\ A_{21} & A_{22} \end{vmatrix} \begin{vmatrix} \phi_C \\ \phi_A \end{vmatrix} \tag{27}$$

We can write system (22) explicitly as

$$F_1(\phi_C, \phi_A) = f_C(\phi_C) - A_{11}\phi_C - A_{12}\phi_A = 0 \tag{28}$$

$$F_2(\phi_C, \phi_A) = f_A(\phi_A) - A_{21}\phi_C - A_{22}\phi_A = 0 \tag{29}$$

The Jacobian matrix J associated with system (28) and (29) is

$$J = \frac{\partial(F_1, F_2)}{\partial(\phi_C, \phi_A)} = \begin{vmatrix} f_C'(\phi_C) - A_{11} & -A_{12} \\ -A_{21} & f_A'(\phi_A) - A_{22} \end{vmatrix} \tag{30}$$

where

$$f_C'(\phi_C) = \frac{df_C}{d\phi_C} \quad \text{and} \quad f_A'(\phi_A) = \frac{df_A}{d\phi_A} \tag{31}$$

Therefore

$$\begin{vmatrix} \phi_C \\ \phi_A \end{vmatrix}_{K+1} = \begin{vmatrix} \phi_C \\ \phi_A \end{vmatrix}_K - J^{-1} \begin{vmatrix} F_1(\phi_C, \phi_A) \\ F_2(\phi_C, \phi_A) \end{vmatrix}_K \tag{32}$$

The iteration proceeds as follows:

(i) Guess ϕ_C^K and ϕ_A^K.
(ii) Calculate $F_1(\phi_C^K, \phi_A^K)$ and $F_2(\phi_C^K, \phi_A^K)$.
(iii) Calculate $f_C'(\phi_C^K)$ and $f_A'(\phi_A^K)$ from the polarization curves. The derivatives can be obtained by a curve-fitting technique, such as cubic splines.[11]
(iv) Form the inverse of the Jacobian matrix.
(v) Find ϕ_C^{K+1} and ϕ_A^{K+1} from (32).
(vi) Repeat steps (i)–(v) until convergence is achieved.
(vii) Calculate ϕ_I from the last row of equation (21): $\phi_I = A_{31}\phi_C + A_{32}\phi_A$.

Satisfying the solvability condition

The analysis of this section verifies that the solvability condition (9) is satisfied in the limit, when convergence occurs. Since the analysis for the three iteration methods is identica, only the case of Jacobi's method is considered.

Jacobi's method can be stated as

$$\begin{vmatrix} A_{11} & A_{12} \\ A_{21} & A_{22} \end{vmatrix} \begin{vmatrix} \phi_C^K \\ \phi_A^K \end{vmatrix} = \begin{vmatrix} f_C(\phi_C^K) - A_{11}(\phi_C^{K+1} - \phi_C^K) \\ f_A(\phi_A^K) - A_{22}(\phi_A^{K+1} - \phi_A^K) \end{vmatrix} \tag{33}$$

and equation (22) states that

$$\begin{vmatrix} A_{11} & A_{12} \\ A_{21} & A_{22} \end{vmatrix} \begin{vmatrix} \phi_C^K \\ \phi_A^K \end{vmatrix} = \begin{vmatrix} q_C^K \\ q_A^K \end{vmatrix} \tag{34}$$

Given a particular value for ϕ_C^K and ϕ_A^K, by solving for q_C^K and q_A^K we are assured that the conservation equation (9) is satisfied, namely,

$$q_C^K \text{ meas}(\Gamma_C) + q_A^K \text{ meas}(\Gamma_A) = 0 \tag{35}$$

But, at the same time, using equation (33) we can rewrite (35) as

$$[f_C(\phi_C^K) - A_{11}(\phi_C^{K+1} - \phi_C^K)] \text{ meas}(\Gamma_C) + [f_A(\phi_A^K) - A_{22}(\phi_A^{K+1} - \phi_A^K)] \text{ meas}(\Gamma_A) = 0 \tag{36}$$

In the limit, when $\phi_C^K \to \phi_C^\infty$ and $\phi_A^K \to \phi_A^\infty$, equation (36) reduces to

$$f_C(\phi_C^\infty) \text{ meas}(\Gamma_C) + f_A(\phi_A^\infty) \text{ meas}(\Gamma_A) = 0 \tag{37}$$

guaranteeing that the constraint equation (9) is satisfied.

Benchmark problems

To validate the significance of the concept of multiple domain and compare the different iterative methods, we

treat three benchmark problems from the corrosion literature.[12-16] In the first two cases, linear boundary conditions are assumed; i.e., the problems can be solved by the direct (noniterative) method. Here, the accuracy of multiple domain is investigated. In the third example, the boundary condition is nonlinear; therefore, both multiple-domain and iterative methods are employed.

Example 1

The geometry under consideration is a rectangular region as shown in *Figure 3*. The anode and the cathode are assumed to have linear polarization functions with equal slopes $L_A = L_C$, which, without loss of generality, are assumed to be unity. These functions are shown in *Figure 5*, and their analytical expressions are

$$\frac{\partial \phi}{\partial n} = \frac{\phi - 1}{L_A} \qquad 0 \leqslant x \leqslant a,\ y = 0 \tag{38}$$

$$\frac{\partial \phi}{\partial n} = \frac{\phi}{L_C} \qquad a \leqslant x \leqslant c \quad y = 0 \tag{39}$$

This problem has been analyzed in Refs. 15 and 16, where the method of separation of variables was used. The analytical solution is

$$\phi(x, y) = a + \frac{2}{\pi} \sum_{n=1}^{\infty} \frac{\sin n\pi a \cos n\pi x \cosh n\pi(b - y)}{n(\cosh n\pi b + n\pi L \sinh n\pi b)} \tag{40}$$

where $L_A = L_C = L = 1$.

The single and 10 images of the rectangular domain are considered for a comparative study. The number of BEM panels on each boundary are assumed to be multiples of 4 (i.e., 4, 8, ..., 40). The case of 40 elements on each boundary for single and multiple domains are shown in *Figure 6* and are compared with the analytical solution (40). Since the differences cannot be observed on this scale, the root-mean-square error for different numbers of elements on each side is depicted in *Figure 7*. As

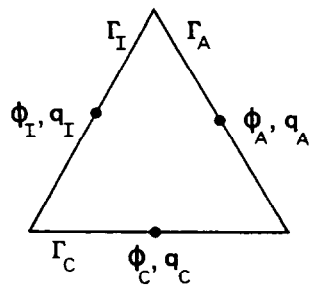

Figure 3 An idealized domain

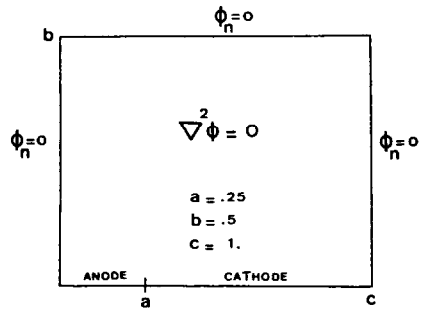

Figure 4 Geometry of Example 1 (linear corrosion problem)

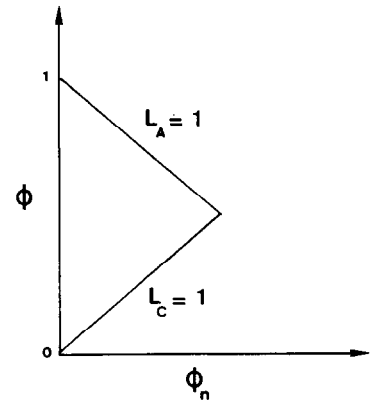

Figure 5 Linear anodic and cathodic polarization curves (linear corosion problem)

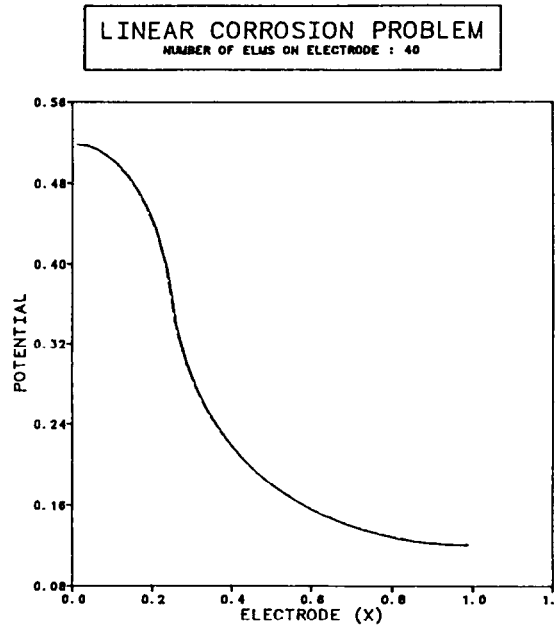

Figure 6 Comparison between different solutions

we can see, the errors are much smaller for the multiple-domain case. The root-mean-square error (RMS) is calculated according to equation (41), where $\hat{\phi}_i$ and ϕ_i are the boundary element and the exact potentials and N is the number of panels on each boundary.

$$\mathrm{RMS} = \frac{1}{N} \sqrt{\sum_{i=1}^{N} (\hat{\phi}_i - \phi_i)^2} \tag{41}$$

Example 2

The geometry of this example is more complicated than Example 1, because the bottom part of the domain is no longer a horizontal line. This boundary is a cosine wave given analytically by (see *Figure 8*)

$$h(x) = 0.15[1 - \cos \pi x] \qquad 0 \leqslant x \leqslant 1 \quad y = 0 \tag{42}$$

The boundary condition associated with this boundary

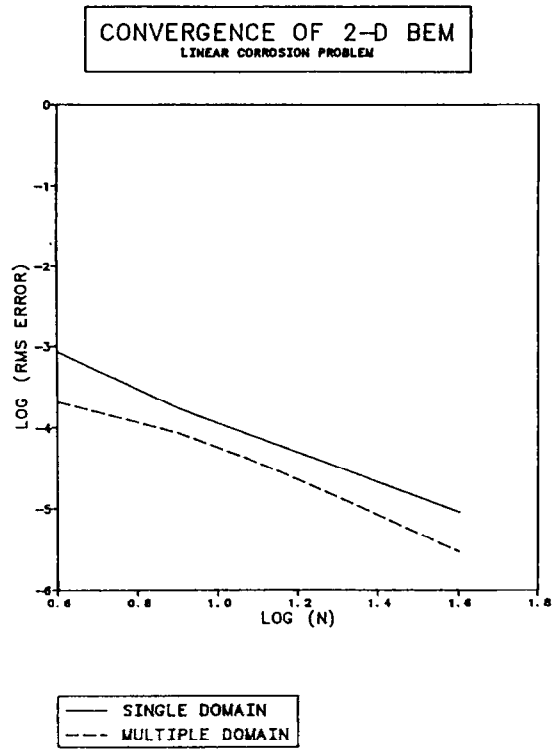

Figure 7 Comparison of RMS errors for single- and multiple-domain cases

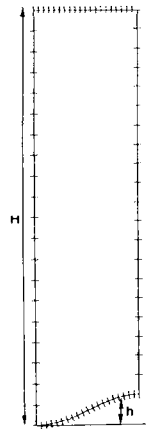

Figure 8 Single domain

is again of linear type and is expressed as

$$\frac{\partial \phi}{\partial n} = f_1 \phi + f_2 \tag{43}$$

where

$$f_1 = -\pi n_x \tan \pi x \tag{44}$$

$$f_2 = -\pi n_y \cos \pi x [e^{-\pi y} - e^{\pi(y-2H)}] \tag{45}$$

The variables n_x and n_y are the components of the outward normal vector to this boundary, and H is the height of the domain in the y-direction. The other three boundary conditions are

$$\phi(x, H) = 0 \qquad 0 \leqslant x \leqslant 1 \quad y = H \tag{46}$$

$$\frac{\partial \phi}{\partial n} = 0 \qquad 0 \leqslant y \leqslant H \quad x = 0 \text{ and } 1 \tag{47}$$

This problem, which has been solved in Ref. 14, has analytical solution

$$\phi(x, y) = \cos \pi x [e^{-\pi y} - e^{\pi(y-2H)}] \tag{48}$$

The treatment of this example, such as the number of images and the number of panels, is exactly as in Example 1 (see *Figures 8* and *9*). Furthermore, again due to the linearity of the boundary value problem, a noniterative method can be employed.

Typical results of 40 elements on each side for single and multiple domains are shown in *Figure 10*. Here, the differences due to the corner singularity can be observed at the extreme left and right sides. The plots of RMS error for single and multiple domains are shown in *Figure 11*, again verifying the advantage of the latter.

Notice that, except for the lower boundary, the major difference between the two examples is the aspect ratio of the two geometries. Therefore, we conjecture that the

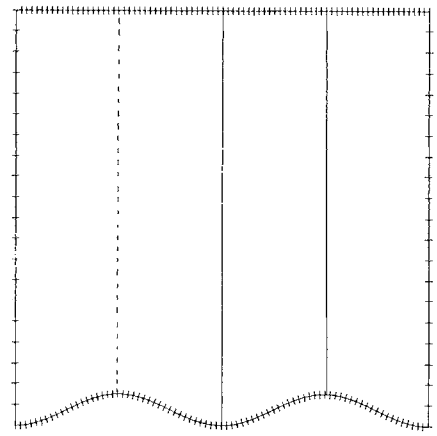

Figure 9 Multiple domain where, due to space considerations, only three images are shown

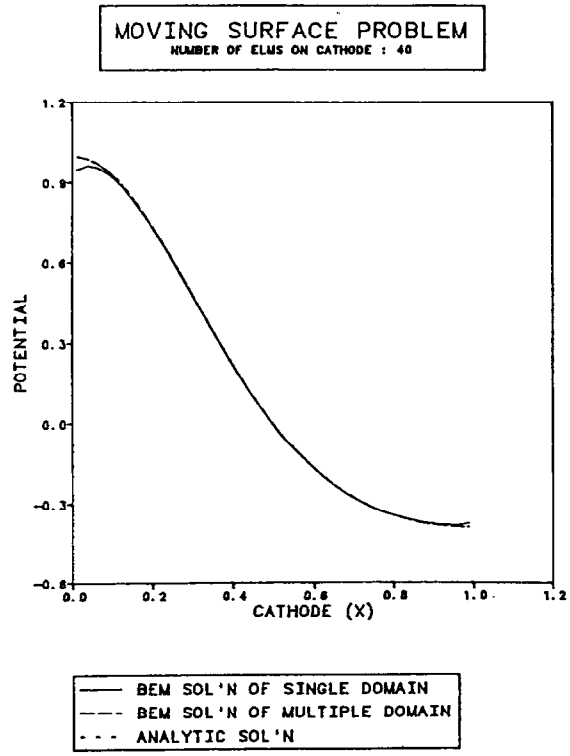

Figure 10 Comparison between different solutions in Example 2

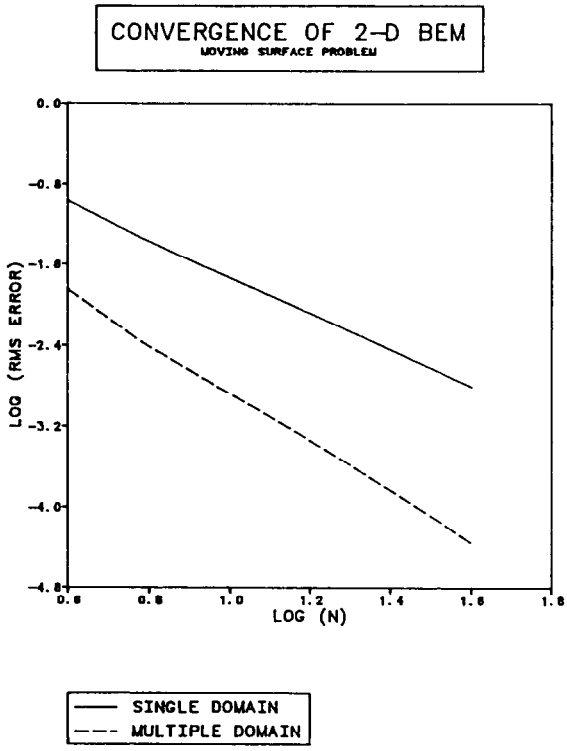

Figure 11 Comparison of RMS errors for the single- and multiple-domain cases of Example 2

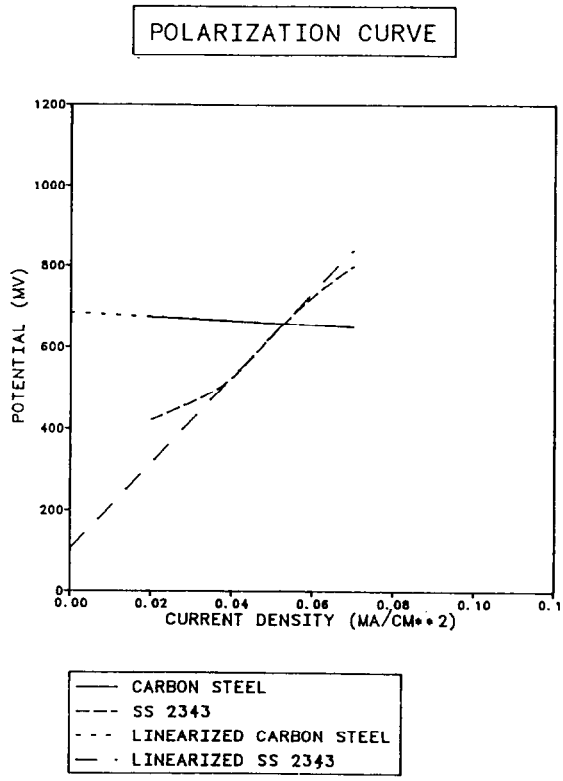

Figure 12 Nonlinear polarization curves along with the linearized approximations

RMS error depends not only on the number of panels but also on the aspect ratio.

Example 3

The domain under consideration is exactly that of Example 1, which is shown in *Figure 4*. The involved dimensions are $a = 20$ cm, $b = 30$ cm, and $c = 40$ cm. The electrolyte is assumed to be homogeneous with a resistivity of $\rho = 22.5$ ohm cm. In this example, the anode and the cathode are assumed to be carbon steel and stainless steel 2343, respectively. The full nonlinear polarization curves for these metals[12] are shown in *Figure 12*. To compare the numerical solutions and assess the iterative methods, we decided to use a linear approximation to the polarization curves for obtaining an exact solution. These linear approximations are also shown in *Figure 12*, and undoubtedly they are well justified. The above linear approximations have open-circuit potentials of $E_A = 685$ mV and $E_C = 105$ mV and polarization parameters of $L_A = 22.22$ cm and $L_c = 466.67$ cm. The reader is reminded that the relationship between current density and flux is $i = \sigma(\partial\phi/\partial n)$. The analytical solution for the linearized problem for $L_A \neq L_C$ is in Refs. 15 and 16. The boundary element solution of the problem, along with some experimental results, is in Ref. 12.

In this article each side of the domain is discretized into 22 panels (elements), and 10 images of the original domain are employed. On the electrodes, two small elements are specified at the left and right sides of the junction in order to account for the discontinuity of the flux.

The convergence criterion defined for the iteration is that the relative difference of the successive solutions at each collocation point (centroid of a panel) must be less than 1.E-10. The comparison of the Jacobi, Gauss–Siedel, and Newton–Raphson methods is shown in *Table 1*.

Table 1 Summary of different iterative methods

Iteration method	Jacobi	Gauss-Siedel	Newton Raphson
Convergence criterion (relative diff)	1.E-10	1.E-10	1.E-10
Number of iterations	679	353	3
RMS error (potential mV)	3.456E-3	3.4567E-3	3.4567E-3
RMS error (current density μA/cm^2)	1.2640E-2	1.2640E-2	1.2640E-2
CPU time (s) (CDC CYBER 825)	19.126	14.99	10.793

The RMS errors in *Table 1* are based on the comparison with the solution of the linearized problem.

The initial guess and the intermediate solutions obtained from the different iterative methods are shown in *Figures 13–15*. *Figure 16* demonstrates the discontinuity of the flux at the junction point for the Newton–Raphson method. The other two methods reproduce the same behavior. Finally, in *Figure 17*, the RMS error is plotted against the number of iterations, where the steep slope of the Neutron–Raphson method verifies its fast rate of convergence.

Conclusions

During the past eight years, there has been much effort in designing CP systems using computer simulations. Presently, several general-purpose CP software packages are available. Among these are packages developed by Computational Mechanics Consultants, Westinghouse Research and Development, and the Defense Research

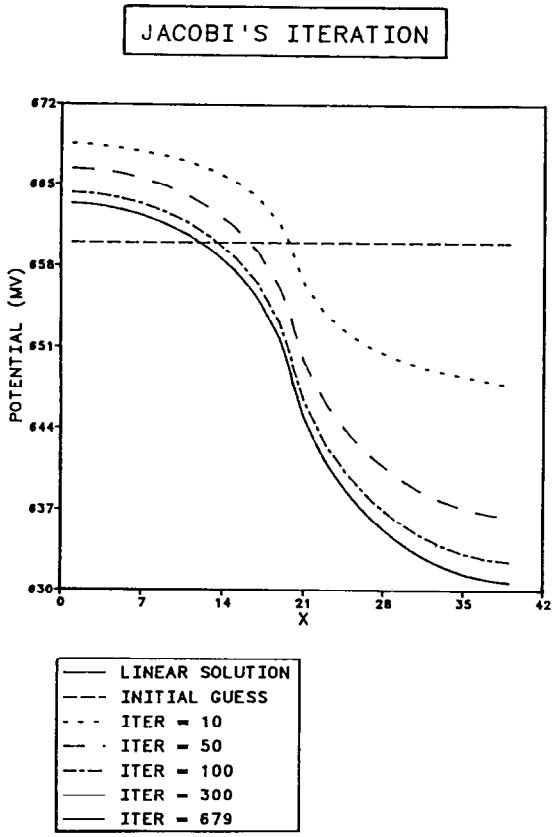

Figure 13 Different iterates for Jacobi's method

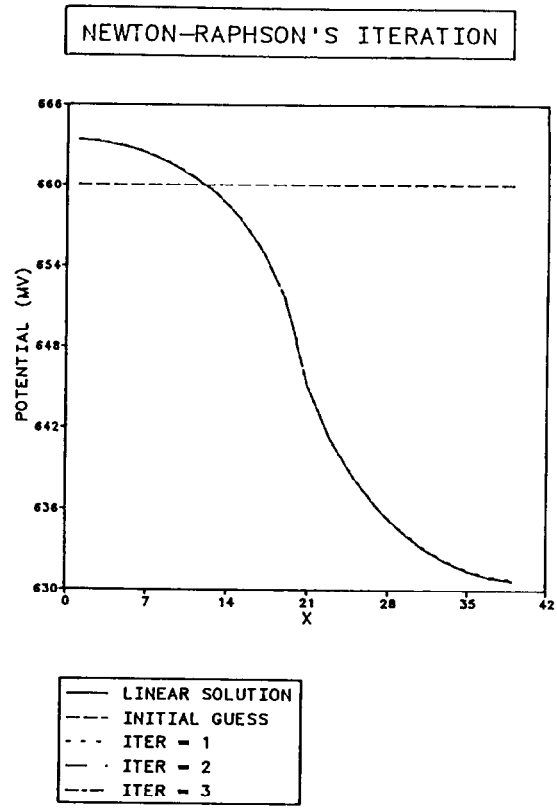

Figure 15 Different iterates for Newton–Raphson method

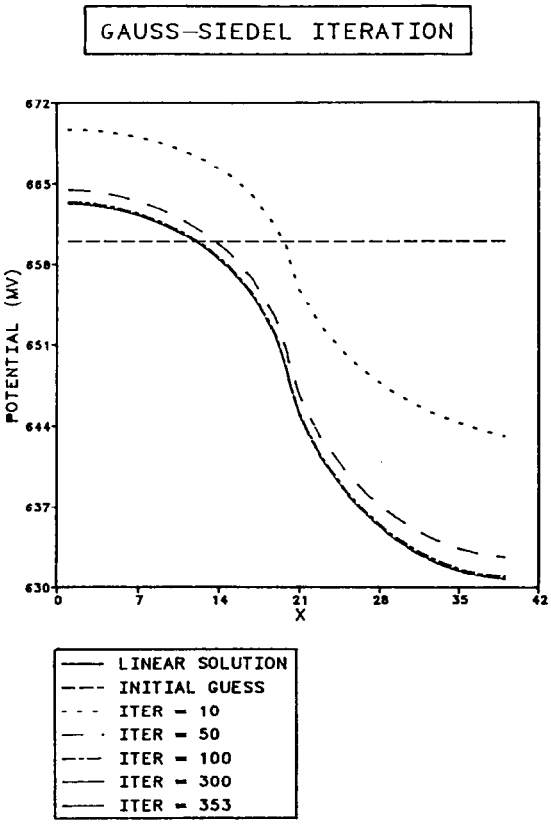

Figure 14 Different iterates for Gauss–Siedel method

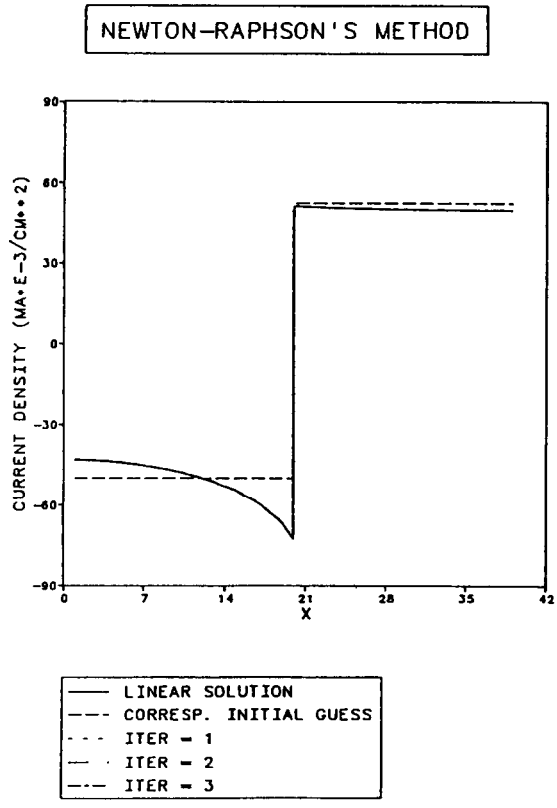

Figure 16 Calculated current density iterates on the anode and the cathode

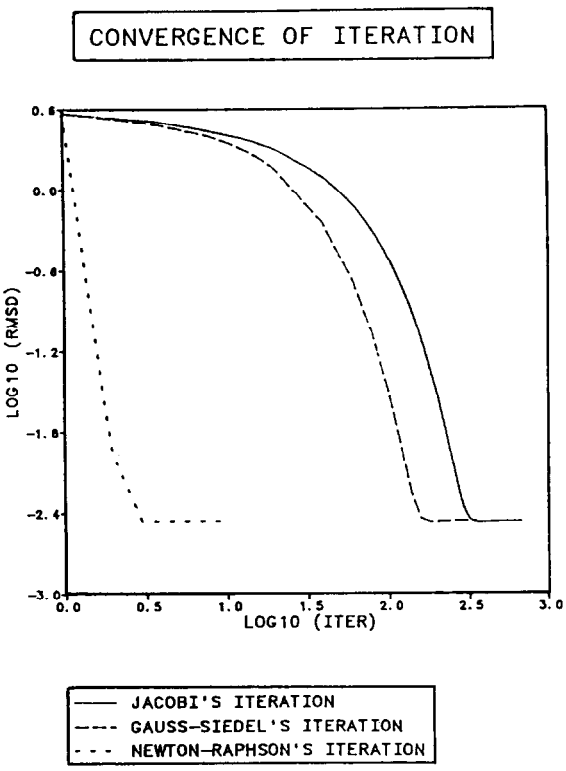

Figure 17 Comparison of the rate of convergence for the different iteration methods

Establishment Atlantic. Some versions of these packages can also run on microcomputers. It is now widely believed that the BEM is the most efficient technique for CP simulation.

This paper has singled out two aspects of CP simulation dealing with the concepts of multiple domain and the iteration procedure to resolve the nonlinearities. The authors have demonstrated that the multiple-domain technique produces more accurate results and should be employed when possible. As far as iterative methods are concerned, the Newton–Raphson method has achieved convergence in very few iterations and can be implemented with minimum effort. Therefore, the combination of the concept of multiple domain and the Newton–Raphson technique seems to be the most effective procedure for boundary element simulation of CP systems.

A final comment is in order. Although the nonlinearities considered here are mild, the authors have looked at more severe nonlinearities of which the results are in Ref. 17.

Acknowledgments

The second author would like to acknowledge the support of Imperial Oil of Canada and NSERC grant A8969.

References

1 Zamani, N. G., Porter, J. F. and Mufti, A. A. A survey of computational efforts in the field of corrosion engineering, *Int. J. Num. Meth. Eng.*, 1986, **23**, 1295–1311
2 Jaswon, M. A. and Symm, G. T. Integral equation methods in potential theory and elastostatics, *Academic Press, New York*, 1977
3 Smirnov, V. I. Integral equations and partial differential equations, a course of higher mathematics, Vol. IV, *Pergamon, London*, 1964
4 Chuang, J. M., Zamani, N. G. and Hsuing, C. C. Numerical simulation of the electroplating phenomenon or reversed corrosion, *Technical Report CADCAMTR-85-06, Technical University of Nova Scotia, October* 1985
5 Chuang, J. M., Zamani, N. G. and Hsuing, C. C. Boundary element methods in electroplating problem, *Proc. Int. Conf. on Boundary Element Technology, BETECH 86, M.I.T., Cambridge, June 1986*
6 Danson, D. J. and Warne, M. A. Current density/voltage calculations using boundary element techniques, *Corrosion 83, Paper No. 211*, 1983
7 Fu, J. W. and Chow, J. S. Cathodic protection designs using an integral equation numerical method, *Corrosion 82, Paper No. 183*, 1982
8 Lamb, H. Hydrodynamics, 6th ed., *Cambridge University Press*, 1945
9 Munn, R. S. Modelling of electrochemical phenomena for finite element analysis of galvanic systems. I. Use of applied current (conduction) boundary conditions, *Naval Underwater Systems Center, TM. No. 831019, New London, Connecticut*, 1983
10 Zamani, N. G. and Peters, F. H. The application of boundary element method in electrodeposition problems, *Appl. Math. Modelling*, 1986, **10**, 262–265
11 Ahlberg, J. H., Nilson, E. N. and Walsh, J. L. The theory of splines and their applications, *Academic Press, New York and London*, 1967
12 Bardal, E. Johnson, R. and Gartland, P. Prediction of galvanic corrosion rates and distribution by means of calculation and experimental models, *NACE*, 1984
13 Helle, H. Beek, G. and Ligtelijn, J. Numerical determination of potential distributions and current densities in multi-electrode systems, *Corrosion*, 1981, **9**, 522–530
14 Hume, E., III, Brown, R. and Deen, W. Comparison of boundary and finite element methods for moving-boundary problems governed by a potential, *Int. J. Num. Meth. Eng.*, 1985, **21**, 1295–1314.
15 Kennard, E. and Waber, J. Mathematical study of galvanic corrosion, equal coplanar anode and cathode with unequal polarization parameters, *J. Electrochem. Soc.* 1970, **117**, 880–885
16 Waber, J. T. and Fogan, B. Mathematical studies on galvanic corrosion. IV. Influence of electrolyte thickness on the potential and current distributions of coplanar electrodes using polarization parameters, *J. Electrochem. Soc.*, 1956, **103**, 64–72
17 Zamani, N. G., Chuang, J. M. and Porter, J. F. BEM simulation of cathodic protection systems employed in infinite electrolytes, *Int. J. Num. Meth. Eng.*, 1987, **24**, 605–620